

# The Formation of Star Patterns on Lake Ice

Victor C. Tsai

March 15, 2007

## 1 Abstract

Star-like patterns have been found on many lakes that have a snow cover on top of a thin ice layer. A number of workers have described these ‘lake stars’ but there have been no attempts at constructing a mathematical model of the formation process. Here we put forth a mathematical model that describes the formation of radial fingers emanating from a central source. Performing linear stability analysis on the steady state solution, we are able to accurately predict the formation of fingers but the number of fingers is very sensitive to input parameters. We also carry out scaled experiments. At small times and to first order, the results of these experiments agree with our linear theory.

## 2 Introduction

It is a common occurrence that snow falls on lakes that already have a thinly ice covered surface. Holes often form in the thin ice (for reasons not well understood [3]), after which warm lake water flows through the hole and through the snow layer. This warm water melts the snow and leaves dark regions where the snow has melted away. The pattern left by this process looks star-like (see Figure 1) and we call this pattern a ‘lake star.’ Lake stars have been described a number of times (e.g. [3, 2, 5]) but very little work has been done to understand the formation process. Knight [3] outlines a physical idea that is meant to describe the process, but no attempt is made at determining whether this idea can be translated into a physical model that produces results consistent with field observation. The main idea of Knight is that locations with faster flow rates melt preferentially, leading to even faster flow rates and therefore to an instability that results in fingers. This idea is qualitatively similar to many other geomorphologic instability such as the ones discussed by Schorghofer et al. [4]. We take this idea as the starting point for our model.

## 3 Mathematical Model

### 3.1 Mathematical Formulation

In order to model the physics of lake star formation, we make a number of assumptions. Many of these assumptions are not strictly true but are reasonable approximations that



Figure 1: Typical lake star pattern. The branched arms are approximately 1 m in length.

facilitate the attainment of a simple solution that can be easily compared with observations. We shall discuss each assumption when it is made.

We begin our analysis by supposing that there exists a central hole through which warm lake water can seep. Both Katsaros [2] and Woodcock [5] attribute these holes as well as the associated lake star patterns to convection patterns within the lake. However, at least in some circumstances the holes seem to be formed from protrusions (e.g. sticks that poke through the ice surface) [3] thus casting doubt on the convection idea. Lake stars are observed in all of these circumstances so we treat the hole formation as independent of, but necessary for, lake star formation. As discussed by Knight [3], the hole results in a water level that extends above the thin ice and into a slush (wet snow) layer. We therefore treat this (warm) water region as having a constant height above the ice or equivalently a constant pressure head. This pressure head drives flow of water through the slush layer, subject to a melting condition (Stefan condition) at the water-slush interface. We treat flow within the slush as a Darcy flow of water at  $0^{\circ}\text{C}$ . Temperature within the liquid region is assumed to obey the (advection-diffusion) heat equation. The water in both the liquid and slush regions is treated as incompressible. In order to fully specify the mathematical problem, we require an outer boundary at which the pressure head is also known. While pressure measurements have not been made in the field, circular water-saturated regions (a few meters in radius) typically surround the lake stars. It therefore seems reasonable to assume that the differential pressure head falls to zero somewhere in the vicinity of this circular boundary. The actual boundary at which the differential pressure head is zero likely is not completely uniform (as in Figure 4 of Knight [3]) but is at least a good approximation especially before strong finger formation (i.e. in the linear regime in which we perform our analysis). Finally, we treat the system as a two-dimensional flow. This cannot be strictly true for two reasons. First, the water in contact with ice must be at  $0^{\circ}\text{C}$  whereas we treat this water as having an average temperature above freezing. However, perhaps this assumption is reasonable in a depth averaged sense. Second, the decreasing pressure head in the radial direction must be accompanied by a corresponding drop in water level, thus

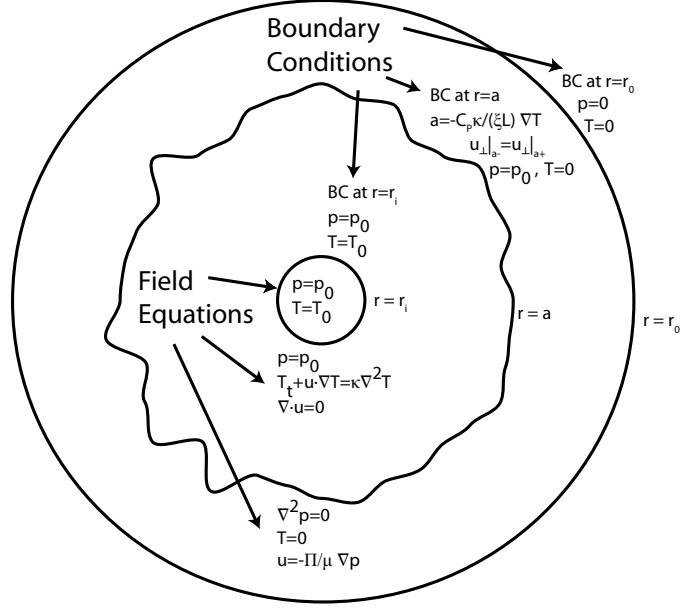


Figure 2: Schematic of the geometry of the model. The perspective is looking down on a nascent star. The equations are shown in the domains of the system and described in more detail below.

making the vertical dimension non-uniform. Therefore, the driving force is more accurately described as deriving from an axisymmetric gravity current. Regardless, the front whose stability we assess is controlled by the same essential physical processes that we model herein. For the purposes of the simple analysis presented here, we shall ignore these two second order effects but note that the analysis could be extended to account for them.

Translating the description in the previous paragraph into mathematical language, we have the following system of equations (see also Figure 2):

$$\frac{\partial T}{\partial t} + \mathbf{u} \cdot \nabla T = \kappa \nabla^2 T \quad r_i < r < a(\phi, t), \quad (1)$$

$$T = 0 \quad a(\phi, t) < r < r_0, \quad (2)$$

$$p = p_0 \quad r_i < r < a(\phi, t), \quad (3)$$

$$\nabla^2 p = 0 \quad a(\phi, t) < r < r_0, \quad (4)$$

$$\nabla \cdot \mathbf{u} = 0 \quad r_i < r < a(\phi, t), \quad (5)$$

$$\mathbf{u} |_{a-} = \mathbf{u} |_{a+} \quad r = a(\phi, t), \quad (6)$$

$$\mathbf{u} = -\frac{\Pi}{\mu} \nabla p \quad a(\phi, t) < r < r_0, \quad (7)$$

with boundary conditions

$$\dot{a} = -\frac{C_P \kappa}{\xi L} \nabla T \quad r = a(\phi, t), \quad (8)$$

$$T = \begin{cases} T_0 & r = r_i \\ 0 & r = a(\phi, t) \\ 0 & r = r_0 \end{cases}, \quad (9)$$

$$p = \begin{cases} p_0 & r = r_i \\ p_0 & r = a(\phi, t) \\ 0 & r = r_0 \end{cases}, \quad (10)$$

where (1) describes advection-diffusion in the liquid, (4) and (5) describe mass conservation with a Darcy flow (7) in the slush, (8) is the Stefan condition, and (9) and (10) are the temperature and pressure boundary conditions, respectively. Note that (3) and (5) can both be satisfied since the liquid region has an effectively infinite permeability.  $T$  is temperature,  $\mathbf{u}$  is Darcy fluid velocity,  $p$  is pressure, and  $a$  denotes the liquid-slush interface. Liquid properties are  $\kappa$  (thermal diffusivity),  $C_P$  (specific heat) and  $\mu$  (dynamic viscosity). Slush properties are  $\Pi$  (permeability),  $\xi$  (solid fraction) and  $L$  (latent heat).

Non-dimensionalizing the equations yields

$$\frac{\partial \theta}{\partial t} + \mathbf{u} \cdot \nabla \theta = \epsilon \nabla^2 \theta \quad r_0 < r < a(\phi, t), \quad (11)$$

$$\theta = 0 \quad a(\phi, t) < r < 1, \quad (12)$$

$$p = 1 \quad r_i < r < a(\phi, t), \quad (13)$$

$$\nabla^2 p = 0 \quad a(\phi, t) < r < 1, \quad (14)$$

$$\nabla \cdot \mathbf{u} = 0 \quad r_i < r < a(\phi, t), \quad (15)$$

$$\mathbf{u}|_{a-} = \mathbf{u}|_{a+} \quad r = a(\phi, t), \quad (16)$$

$$\mathbf{u} = -\nabla p \quad a(\phi, t) < r < 1, \quad (17)$$

with boundary conditions

$$\dot{a} = -\frac{\epsilon}{S} \nabla \theta \quad r = a(\phi, t), \quad (18)$$

$$\theta = \begin{cases} 1 & r = r_i \\ 0 & r = a(\phi, t) \\ 0 & r = 1 \end{cases}, \quad (19)$$

$$p = \begin{cases} 1 & r = r_i \\ 1 & r = a(\phi, t) \\ 0 & r = 1 \end{cases}, \quad (20)$$

where all variables are now non-dimensional with length, velocity, pressure and temperature scaled (respectively) by

$$l \sim r_0, \quad (21)$$

$$U \equiv u_0 \sim \frac{\Pi p_0}{\mu r_0}, \quad (22)$$

$$P \sim p_0, \quad (23)$$

$$T \sim T_0 \quad T = T_0 \theta, \quad (24)$$

and non-dimensional parameters  $\epsilon$  and  $S$  are given by

$$\epsilon \equiv \frac{\kappa}{u_0 r_0}, \quad (25)$$

$$S \equiv \frac{\xi L}{C_P T_0}. \quad (26)$$

In the lake star system, liquid temperatures must be less than or equal to 4°C since the lake is frozen at the top. Making conservative estimates,  $T_0 < 4^\circ\text{C}$ ,  $\xi > 0.3$  and  $L/C_P \approx 80^\circ\text{C}$  then  $S > 6 \gg 1$ . Estimating  $u_0$  ( $1\text{cm/hr} < u_0 < 10\text{cm/hr}$ ) and  $r_0$  ( $0.3\text{m} < r_0 < 3\text{m}$ ) from the field observations of Knight [3] and using  $\kappa \approx 10^{-7}\text{m}^2\text{s}^{-1}$  yields  $\epsilon < 0.1 \ll 1$ . Assuming  $S \gg 1$  (quasi-stationary approximation, which we adopt henceforth) and  $\epsilon \ll 1$ , equations (11) - (20) are easily solved for a purely radial flow with cylindrical symmetry (no  $\phi$  dependence) and circular liquid-slush interface. This (boundary layer) solution is

$$\mathbf{u} = u\hat{r} = -\frac{1}{\log(a_0)} \frac{1}{r} \hat{r} \quad r_i < r < 1, \quad (27)$$

$$p_b = \frac{\log(r)}{\log(a_0)} \quad r > a_0, \quad (28)$$

$$\theta_0 = 1 - \left(\frac{r}{a_0}\right)^{\frac{1}{\epsilon}(-1/\log(a_0)+2\epsilon)} \quad r < a_0, \quad (29)$$

$$\frac{S a_0 \dot{a}_0}{-1/\log(a_0) + 2\epsilon} = 1, \quad (30)$$

where equation (30) has an approximate implicit solution for  $a_0$  given by

$$\frac{a_0^2}{4} - \frac{1}{2} a_0^2 \log(a_0) = \frac{t}{S}. \quad (31)$$

### 3.2 Linear Stability Analysis

In order to study the growth of perturbations from steady state, we perform a linear stability analysis around this cylindrically symmetrical flow. In this linear approximation, we still have a purely radial flow since the azimuthal component of flow enters quadratically with perturbations from steady state. Setting

$$r = a_0 + \epsilon r', \quad (32)$$

$$\phi = \epsilon\phi', \quad (33)$$

$$\theta = \theta_0 + f(r')e^{ik'\phi' + \sigma t}, \quad (34)$$

$$a = a_0 + \epsilon g e^{ik'\phi' + \sigma t}, \quad (35)$$

we first solve (14) subject to (20). For  $g \ll 1$  and  $\epsilon \ll k'$  then

$$p = \frac{\log(r)}{\log(a_0)} + \frac{g \exp(ik'\phi' + \sigma t)}{-a_0 \log(a_0)} \left(\frac{r}{a_0}\right)^{-k'/\epsilon} \quad r > a_0, \quad (36)$$

so that

$$u = \frac{1}{-\log(a_0)} \cdot \frac{1}{r} + \frac{k'}{\epsilon} \cdot \frac{g \exp(ik'\phi' + \sigma t)}{-a_0 \log(a_0)} \left(\frac{r}{a_0}\right)^{-k'/\epsilon - 1} \quad r > a_0. \quad (37)$$

Substituting (37) into (16) and satisfying (15) yields

$$u = \frac{1}{-\log(a_0)} \cdot \frac{1}{r} + \frac{k'}{\epsilon} \cdot \frac{g}{-r \log(a_0)} \exp(ik'\phi' + \sigma t) \quad r < a_0. \quad (38)$$

Substituting (38) into (11), and dropping terms of  $O(\epsilon)$  gives

$$f'' - \frac{1}{-a_0 \log(a_0)} \zeta^{-1} f' - \frac{k'^2}{a_0^2} f = \frac{k'g}{-a_0 \log(a_0)} \zeta^{-1} \frac{\partial \theta_0}{\partial r'} \quad (39)$$

where  $\zeta \equiv r/a_0 = 1 + \epsilon r'/a_0$ , with boundary conditions given by

$$f(r' = -\infty) = 0, \quad (40)$$

$$f(r' = g e^{ik'\phi' + \sigma t}) = 0. \quad (41)$$

To first order in  $g$ , (41) is equivalent to

$$f(r' = g) = -g \frac{\partial \theta_0}{\partial r'}. \quad (42)$$

Solving (39) subject to (40) and (42) gives

$$f(r') = \frac{g}{-a_0 \log(a_0)} \left(1 - \frac{a_0}{-k' \log(a_0)}\right) e^{\lambda^+ r'} + \frac{g}{k' \log^2(a_0)} e^{r'/(-a_0 \log(a_0))}, \quad (43)$$

with

$$\begin{aligned} \lambda^+ &\equiv \frac{1}{2a_0} \left( \frac{1}{-\log(a_0)} + \epsilon + \sqrt{\left(\frac{1}{-\log(a_0)} + \epsilon\right)^2 + 4k'^2} \right) \\ &\approx \frac{1}{-2a_0 \log(a_0)} \left( \sqrt{1 + \frac{4k'^2}{\log^2(a_0)}} + 1 \right) \end{aligned} \quad (44)$$

Equation (18) can be rewritten as

$$\dot{a} = \frac{1}{S} \frac{\partial \theta}{\partial r'} \Big|_{r'=g \exp(ik'\phi' + \sigma t)}, \quad (45)$$

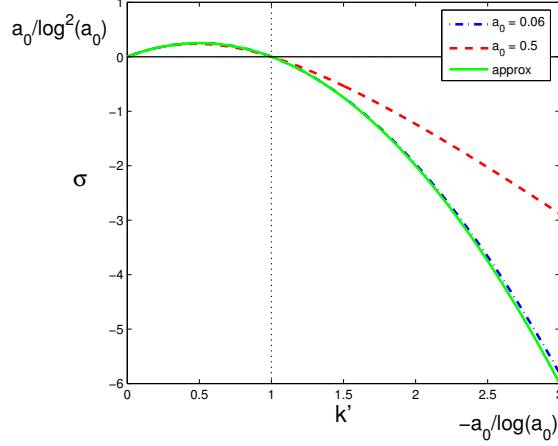


Figure 3: Stability curve: Nondimensional growth rate  $\sigma$  versus nondimensional wavenumber  $k'$ . Scales for the axes are given at the upper left ( $\sigma$  axis) and the lower right corners ( $k'$  axis).  $\sigma$  is plotted for the range of plausible  $a_0$  (blue and red curves) and for the approximation (47) (green curve).

so that substituting (43) into (45) gives the nondimensional growth rate ( $\sigma$ ) as a function of wave number ( $k'$ ):

$$\sigma = \frac{1}{2a_0 \log^2(a_0)S} \left( \sqrt{1 + 4k'^2 \log^2(a_0)} - 1 \right) \left( \frac{a_0}{-k' \log(a_0)} - 1 \right). \quad (46)$$

Equation (46) can be approximated in  $0 \leq x \lesssim 1$  as

$$\sigma \approx \frac{a_0}{\log^2(a_0)S} x(1-x), \quad (47)$$

where  $x \equiv -k' \log(a_0)/a_0$ .

The stability curve (46) and the approximation (47) are plotted in Figure 3. The essential features of (46) are a maximum in the range  $0 < k' < a_0/\log(a_0)$ , zero growth rate at  $k' = a_0/\log(a_0)$  and a linear increase in stability with  $k'$  for large  $k'$ . The maximum growth rate occurs at approximately

$$k'_{max} \approx \frac{a_0}{-2 \log(a_0)}, \quad (48)$$

with (nondimensional) growth rate

$$\sigma_{max} \approx \frac{a_0}{4S \log^2(a_0)}. \quad (49)$$

Translating (48) and (49) back into dimensional quantities, we find that the most unstable mode has angular size given by

$$\phi_{degrees} = \frac{720^\circ \kappa}{u_0 r_0} \left( \frac{r_0}{a_0} \right) \log \left( \frac{r_0}{a_0} \right), \quad (50)$$

and has growth rate given by

$$\sigma_{dim} = \frac{u_0}{4Sr_0 \log^2(r_0/a_0)} \left( \frac{a_0}{r_0} \right). \quad (51)$$

### 3.3 Numerical Results

For observed lake stars, some of the relevant parameters are not well constrained. A plausible guess for  $r_0$  is the radius of the wetted (snow) region around the lake stars since it is a reasonable estimate that if there were significant excess pressure at this point then the wetting front would have advanced further. Field observations [3, 5, 2] constrain this wetted radius to be  $1.5\text{m} \lesssim r_0 \lesssim 4\text{m}$ . However, it is also possible that the effective value of  $r_0$  ( $r_0^{eff}$ ) is less than this either because the wetted radius is smaller earlier in the star formation process or because the ambient pressure level is reached prior to reaching the wetting front. The most logical interpretation of  $a_0$  is either as the radius of the lake star ( $r_{lakestar}$ ) or as the radius of the roughly circular liquid-filled region at the center of the lake star ( $r_{liquid}$ ) (see Figure 4). From field observations [3, 5, 2]  $1\text{m} \lesssim r_{lakestar} \lesssim 2\text{m}$  and  $0.1\text{m} \lesssim r_{liquid} \lesssim 0.5\text{m}$ . Although  $r_0$ ,  $r_{lakestar}$  and  $r_{liquid}$  each have a substantial range, the ratios  $r_{lakestar}/r_0$  and  $r_{liquid}/r_0$  are observed to have a somewhat smaller range of values:  $0.3 \lesssim r_{lakestar}/r_0 \lesssim 0.6$  and  $0.07 \lesssim r_{liquid}/r_0 \lesssim 0.15$ . These constraints are useful since equations (50) and (51) are more sensitive to  $a_0/r_0$  than  $a_0$  or  $r_0$  independently. Here we take  $a_0 \approx r_{liquid}$  as the appropriate value of  $a_0$  during the initial stages of star formation, although perhaps  $r_0^{eff}$  is sufficiently less than  $r_0$  that  $r_{lakestar}/r_0$  is a better approximation to  $a_0/r_0^{eff}$  than  $r_{liquid}/r_0$ . Knight [3] estimates the rate of advance of the wetting front to be somewhat less than 10cm/hr. If the interpretation of  $r_0$  above is correct then this rate gives a reasonable estimate of  $u_0$  as  $1.4 \cdot 10^{-5}\text{m/s} \lesssim u_0 \lesssim 2.8 \cdot 10^{-5}\text{m/s}$ .  $\kappa$  is well constrained by measurements to be  $\kappa \approx 10^{-7}\text{m}^2\text{s}^{-1}$ .

Using these parameter values, our linear theory predicts the most unstable mode to have wavelength between  $8^\circ$  and  $130^\circ$ . Letting  $N$  equal the number of branches, then  $N = 360^\circ/\phi_{deg}$  so that we expect between three and 45 branches (initially). These values of  $N$  encompass the observed values for lake stars ( $4 < N < 15$ ), although the largest values ( $15 < N < 45$ ) are never observed. Despite the dearth of field observations, we are encouraged by many qualitative features such as the fact that stars with larger values of  $a_0/r_0$  seem to have a larger number of branches. Additionally, our analysis predicts that (given constant  $a_0/r_0$ ) larger values of  $r_0$  and  $u_0$  would result in more branches. Larger  $p_0$  (higher water height within the slush layer) and larger  $\Pi$  (less well-packed snow) would result in larger values of  $u_0$ . Thus, some of the variability among field observations is likely to be due to variations in these quantities (for which we have no direct observations).

At this point, it is worth restating the fact that the theory presented here is only a linear one and the phenomenon of lake stars is highly non-linear since the dendritic arms are far from small perturbations to a radially symmetric pattern. Since the non-linear growth phase is likely different from the linear one, it should not be surprising that our model results only approximately agree with observations. In order to more accurately predict observations, one could perform a weakly non-linear pattern formation analysis (e.g. as in Cross and Hohenberg [1]) (which may result in a Landau-type equation) or one could solve the system numerically. Both of these approaches would likely yield improved results.

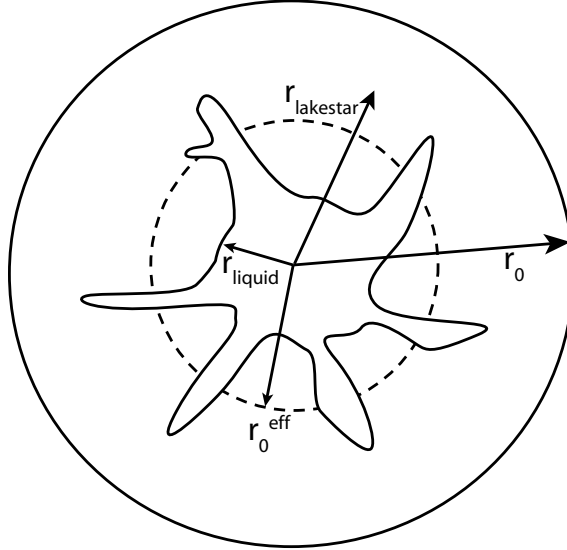


Figure 4: Schematic showing  $r_0$ ,  $r_0^{eff}$ ,  $r_{lakestar}$  and  $r_{liquid}$ .

However, while it is true that a more complex physical model may provide more detailed predictions than the model developed here, the state of the field observations does not at this time warrant that level of detail.

## 4 Experimental Setup

To check the validity of our analysis, we perform laboratory experiments. The goal of these experiments is more to test the conceptual ideas in our simple mathematical model than to make a quantitative connection with the observed lake stars. In these experiments, we cool a circular plate to slightly below freezing ( $\approx -0.5^\circ\text{C}$ ); place a 0.5 to 1-cm high, roughly circular layer of slush on top; and flow  $1^\circ\text{C}$  water through the slush (see Figure 5).

To simulate wet snow we place ice in a high-power blender until the slush is visually uniform, although there is inevitably a range of grain sizes. To form the circular layer of slush we hand-pack the slush directly on the cold circular plate. We attempt to form a constant thickness, roughly circular layer simply by molding the slush and removing excess slush until the correct geometry remains. During this process air bubbles are sometimes incorporated which causes the slush permeability to be variable. This variable permeability likely affects our quantitative results.

We perform the experiment 14 times. The parameters that we vary are the initial size of the water-filled central hole ( $a_0$ ), the initial size of the circular slush layer ( $r_0$ ), and the flow rate ( $Q$ ) (which determines  $u_0$ ). In each run an attempt is made to manually vary the flow rate so that the water level ( $h_0$ ) in the central hole remains roughly constant. In many of the runs, we begin the experiment without the central hole. In practice, however, the first few drops of warm water create a circular hole with radius one to three times the radius of the nozzle that delivers the water ( $0.5\text{cm} < a_0 < 1.0\text{cm}$ ). It is significantly more



Figure 5: Experimental Setup: A 30 cm diameter plate with a built in manifold is connected to a cooling reservoir and maintained within a degree of freezing. A separate reservoir of fresh water 1° above freezing delivers fresh water at 1°C to the center.

difficult to prepare a uniform (permeability) sample with a circular hole initially present. These runs are therefore more difficult to interpret.

We observe fingering of some type in every experimental run. From this we can conclude that fingers are a robust feature under the conditions provided. However, there seem to be two distinct types of fingering: small-scale fingering (see Figure 6) that forms soon after the start of the experiment, and larger channel-like fingers (see Figure 7) that are ubiquitous at later times of the experiment and often extend from the central hole to the outer edge of the slush. Since the channel-like fingers provide a direct path for water to flow (without Darcy flow within the slush), these are likely not directly analogous with lake star fingers. The initial small-scale fingering, on the other hand, have characteristics more like the lake stars. We therefore assume that these small-scale features are the ones of interest. One should note, however, that the larger channel-like fingers seem to form out of small-scale fingers, so there may be a continuum of finger-like features and it is likely that the channels represent a very non-linear growth of the small-scale figures. In each experiment we measure  $a_0$ ,  $r_0$ ,  $h_0$ ,  $Q$ , and distance between fingers ( $d_f$ ), which we tabulate in Table 1. From these quantities, we can calculate  $u_0 = Q/(2\pi r_0 h_0)$ ,  $\phi_{calc} \equiv \phi_{degrees}$  [from equation (50)] and  $\phi_{obs} = 180^\circ d_f/(\pi a_0)$ , and therefore compare scaled experiments both with the model and field observations.

## 5 Comparison of Theory, Experiment and Field Observations

In Figure 8 we plot  $\phi_{obs}$  versus  $\phi_{calc}$  for the various field observations for which we have estimates of parameters, the laboratory experiments described above, and the model [equation



Figure 6: Typical experimental run where small-scale fingers are present. For scale, the nozzle head has diameter of 5 mm.

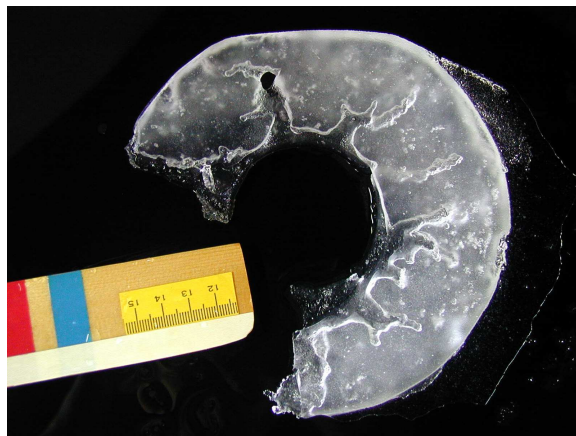


Figure 7: Typical run where channels form. This picture is taken from the underside. Note: part of the slush broke off when it was flipped to image it. The numbers on the ruler are in cm.

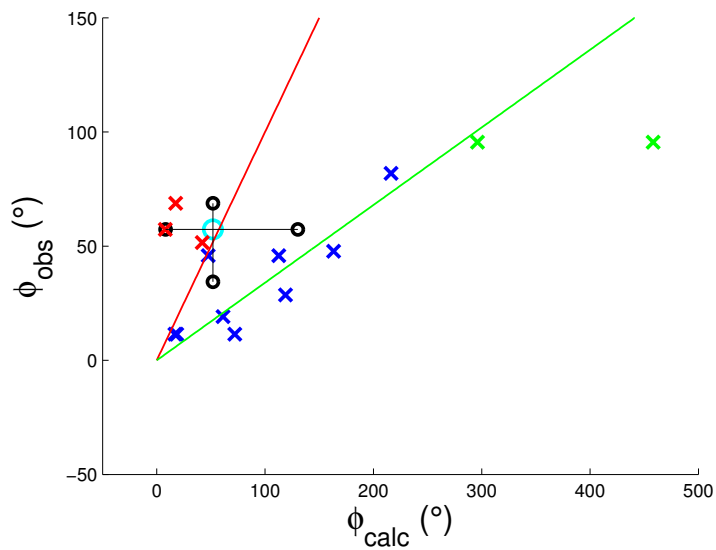


Figure 8: Comparison of theory, experiment and field observations. Circles are field observations (cyan = best constrained field observation, black = range of plausible field observations), crosses are experimental results (red: flag = 1, green: flag = 2, see Table 1), red line is theory, green line is best-fit line of unflagged (blue) experimental results. Note: all experimental results have error bars of at least a factor of two in the x-coordinate and 30% in the y-coordinate (see Table 1).

Expt #	$a_0$ (cm)	$r_0$ (cm)	$h_0$ (mm)	$Q$ (ml/min)	$d_f$ (cm)	flag
1	1.0	8	3	29	0.8	0
2	1.0	8	3	11	0.5	0
3	0.5	10	2	9	1.0	2
4	1.5	10	3	14	0.3	0
5	1.5	9	3	14	0.5	0
6	2.5	8.5	10	143	2.5	1
7	2.5	10	10	86	3.0	1
8	0.7	10	3	14	1.0	0
9	0.5	4.5	3	14	0.4	0
10	1.0	9	10	128	0.9	1
11	2.0	10.5	10	128	0.4	0
12	1.0	3.5	10	71	0.2	0
13	0.3	7.5	3	14	0.5	2
14	0.6	7	3	14	0.5	0

Table 1: Experimental Results: Runs with flag = 1 seem to have channels but show no clear small-scale fingers. In these cases, channel spacing is taken for  $d_f$ . Runs with flag = 2 were not well documented (blurry photos) and therefore difficult to interpret. Errors are approximately 0.3 cm, 0.5 cm, 2 mm, 5 ml/min and 0.2 cm (respectively) for the five measured quantities.

(50)]. The most obvious feature of Figure 8 is the large amount of scatter in both the experimental and observational data. Moreover, the data does not lie on the one-to-one curve predicted by the model. However, the data are not orders of magnitude off from the model predictions, and the experimental results even trend in the right direction, having a best-fit slope of 0.34. We also attempt to find trends in the experimental data not represented by the model by comparing  $y \equiv \phi_{obs}/\phi_{calc}$  vs. various combinations of control parameters ( $\equiv x$ ) including  $r_0$ ,  $a_0$ ,  $r_0/a_0$ ,  $r_0u_0$ ,  $r_0/a_0 \log(r_0/a_0)$  and  $\log(r_0/a_0)/(a_0u_0)$ . For all plots of  $y$  vs.  $x$ , our model predicts a zero slope (and y-intercept of 1). A non-random dependence of  $y$  on  $x$  would point to failure of some part of our model. Thus, to test the validity of our model, we perform significance tests on all non-flagged data with the null hypothesis being a non-zero slope. In all cases, the null hypothesis is accepted (not rejected) at the 95% confidence level. Thus, although the agreement is far from perfect, the simple model captures all of the significant trends in the experimental data.

## 6 Conclusions

By quantifying and extending the qualitative ideas of Knight [3], we have constructed a mathematical model that is able to explain the radiating finger-like patterns on lake ice that we call the lake stars. The model yields a prediction for the wavelength of the most unstable mode as a function of various physical parameters [equation (50)] that agrees decently with field observations. We also perform experiments in which we observe a similar fingering pattern. To first order, the experimental results also agree with the model, although there

is substantial scatter in the data. The disagreement between field observations, model, and experiment can be attributed to poor measurements and the limitations of the simple theory, as discussed in more detail in Sections 3.3 and 4. We expect that adding complexity to the model should yield better quantitative results but that the general idea of the model and the qualitative predictions that result from it should remain valid.

## 7 Acknowledgements

Thanks to John Wettlaufer for guidance, Keith Bradley for help in the lab, the GFD staff for helpful conversations, and all the GFD fellows for a wonderful summer.

## References

- [1] M. C. CROSS AND P. C. HOHENBERG, *Pattern-formation outside of equilibrium*, Rev. Modern Phys., 65 (1993), pp. 851–1112.
- [2] K. B. KATSAROS, *Convection patterns in a pond*, Bull. Amer. Meteor. Soc., 64 (1983), pp. 277–279.
- [3] C. A. KNIGHT, *Slush on lakes*, in Structure and dynamics of partially solidified systems, D. E. Loper, ed., Martinus Nijhoff, Dordrecht, 1987, pp. 453–465.
- [4] N. SCHÖRGHOFER, B. JENSEN, A. KUDROLLI, AND D. H. ROTHMAN, *Spontaneous channelization in permeable ground: theory, experiment, and observation*, J. Fluid Mech., 503 (2004), pp. 357–374.
- [5] A. H. WOODCOCK, *Melt patterns in ice over shallow waters*, Limnol. Oceanogr., 10 (1965), pp. R290–R297.